On the selection of extension twin variants with low Schmid factors in a deformed Mg alloy

Zhang-Zhi Shi, Yudong Zhang, Francis Wagner, Pierre-Alexandre Juan, Stéphane Berbenni, Laurent Capolungo, Jean-Sébastien Lecomte, Thiebaud Richeton

Evolution and selection of twin variants with low Schmid factors in a deformed Mg alloy

Zhangzhi Shi[a], Yudong Zhang[a], Francis Wagner[a], Pierre A. Juan[b], Stéphane Berbenni[a], Jean S. Lecomte[a], Laurent Capolungo[b], Thiebaud Richeton[a]

[a]Laboratoire d'Etude des Microstructures et de Mécanique des Matériaux, LEM3, CNRS 7239, Université de Lorraine U.L. – Metz, Ile du Saulcy, 57045 Metz, France

[b]George Woodruff School of Mechanical Engineering, Georgia Institute of Technology Lorraine, UMI 2958 Georgia Tech–CNRS, 57070 Metz, France

Abstract

Samples of Mg AZ31 alloys were deformed in compression to initiate {10−12} extension twinning. The twins are classified into four types according to their normal strain components along sample axes, in which "Type B" twins, closest to the external strain conditions, appear with the highest frequency. They predominate in grains containing only one twin variant, while the frequencies of other types increase in grains containing more variants. The majority of low Schmid factor (SF) twins with SF ratios ≤ 0.5 are "Type A or D" twins. Based on the concept of displacement gradient tensor, a method is developed to evaluate the strain induced by a twin (i.e., strain applicator) onto five common deformation systems of a high SF twin or the matrix (i.e., strain receiver) in its neighboring grain. It reveals that the selected low SF (even negative) twin variant requires less accommodation through pyramidal slip with high critical resolved shear stress (CRSS), but more accommodation through prismatic or basal slip with low CRSSs in the strain receiver. The formation of these twins contribute to local strain compatibility in the vicinity of grain boundaries.

1. Introduction

{10−12} twinning is an important deformation mode in Mg and its alloys. Since this twinning mode has the second lowest critical resolved shear stress (CRSS) next to that of the basal dislocation slip [1, 2], the {10−12} twins form abundantly under an extension stress along the grains c-axes, which can lead to substantial strain softening [2-6]. Previous studies on the {10−12} extension twinning revealed that their formation approximately obeyed the Schmid factor (SF) rule [7-11]. This rule of twin variants selection favors the twins for which the applied stress resolved onto the twinning plane and in the direction of the

twinning shear is the highest. However, anomalous extension {10−12} twins formed under an external stress imposing compressive strain along the grains c-axes have also been reported [6, 12, 13]. They can form either during loading [13] or during unloading after deformation [14]. Moreover, the SF rule also failed when multiple twin variants were observed, some of which had much smaller SFs than the other possible twin variants [15]. Their formation was attributed to complex internal stress state induced by pre-formed twins and the interaction between slip, twinning and grain boundaries, triple junctions.

Recently, Jonas et al. [16] and Mu et al. [17] revealed that the requirement of the activation of prismatic slip played an important role in twin variants selection in Mg alloys. They used the displacement gradient tensor [16] to analyze the shear accommodation in one grain, which was induced by twins in its neighboring grain. Each non-diagonal component of the accommodation distortion tensor was physically interpreted in terms of slip or twinning. It was found that only the component associated with prismatic slip revealed a noticeable trend, which suggested that the twin variants requiring substantive prismatic slip were absent [16, 17]. In this paper, the evolution of {10−12} extension twin variants is studied. Special attention is paid to the selection of twin variants with low and even negative SFs.

2. Experimental procedure

Specimen are hot rolled sheets of commercial AZ31 alloy (Mg-3Al-1Zn in wt%). The rolling, transverse and normal directions of the rolled sheet are defined as RD, TD and ND, respectively. Cubic specimen with a length of 10 mm were cut for uniaxial compression tests along RD. Compressions stopped at various engineering strains were performed at room temperature with initial strain rate of $1\times10^{-3}s^{-1}$. The present analysis is focused on the compressed specimen with 2.75% of compression strain. For microstructure analysis, the samples were grinded using SiC paper with grit from 2400 to 4000 and then electrolytically polished in an electrolyte of 62.5% phosphoric acid and 37.5% ethanol at 3 V for 30 s and then at 1.5 V for 2 min, at −15 °C. The electron backscatter diffraction (EBSD) measurements were performed using a JEOL 6500F FEG SEM microscopic with Channel 5 analysis system (Oxford HKL). The step size adopted for EBSD measurements is 0.1 μm. This spatial resolution is chosen to allow enough details for twinning detection.

3. Microstructure observations

Fig. 1a displays an EBSD ND inverse pole figure micrograph showing the initial microstructure of the alloy. It is seen that the material is recrystallized, without initial twin. The average grain size is 11.4 μm. Fig. 1b shows the EBSD {0001} pole figure of the initial material. As shown in the figure, the basal pole of the sample is centered around the ND, indicating a typical basal texture of rolled Mg sheets. This texture is favorable for {10−12} extension twinning for loading along RD. For the compressed specimen, the dimensions change in RD, TD and ND is −0.25 mm, 0.05 mm and 0.10 mm, respectively (negative sign means contraction). A typical microstructure of the deformed specimen, presented in EBSD orientation micrograph, is given in Fig. 1c. All the twins are detected to be primary {10−12} extension twins (designated as ETWs). In this figure, about 24% of the total area corresponds to twins and about 84% of the twinned area corresponds to twins connected by another twin at grain boundaries.

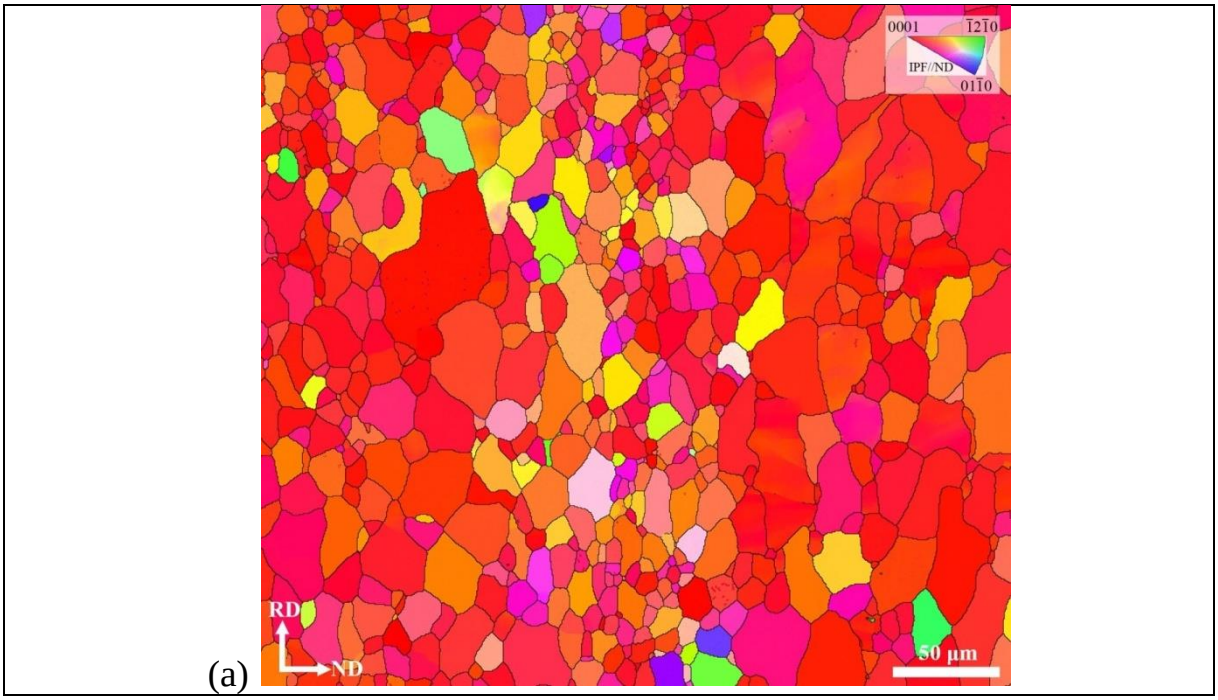

(a)

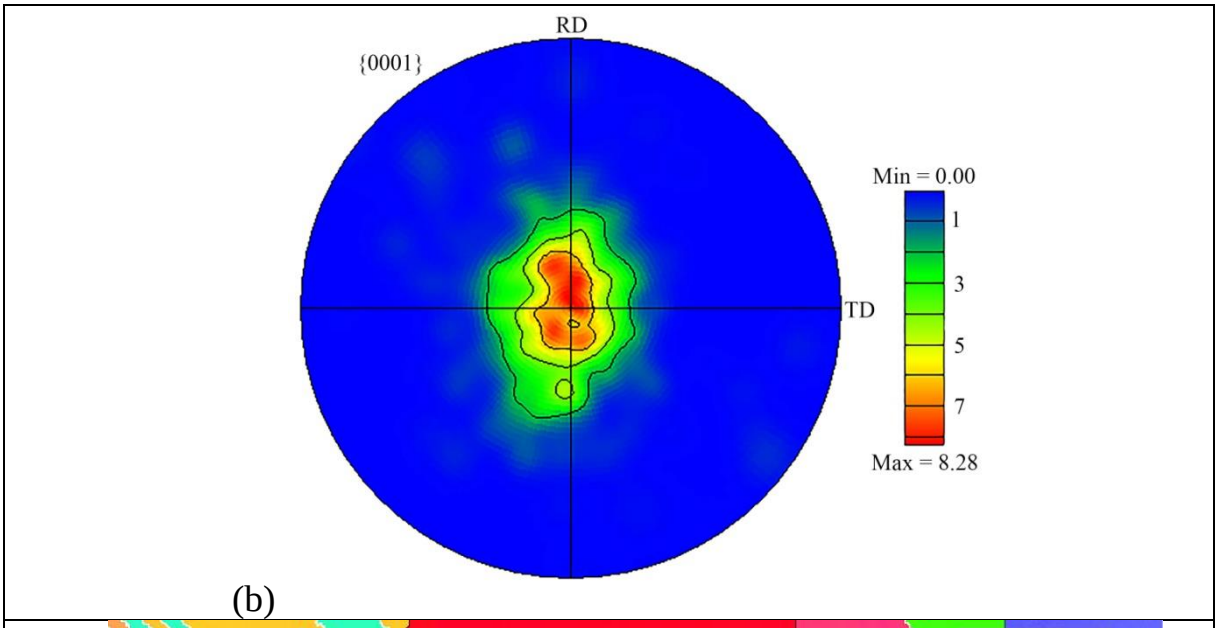

(b)

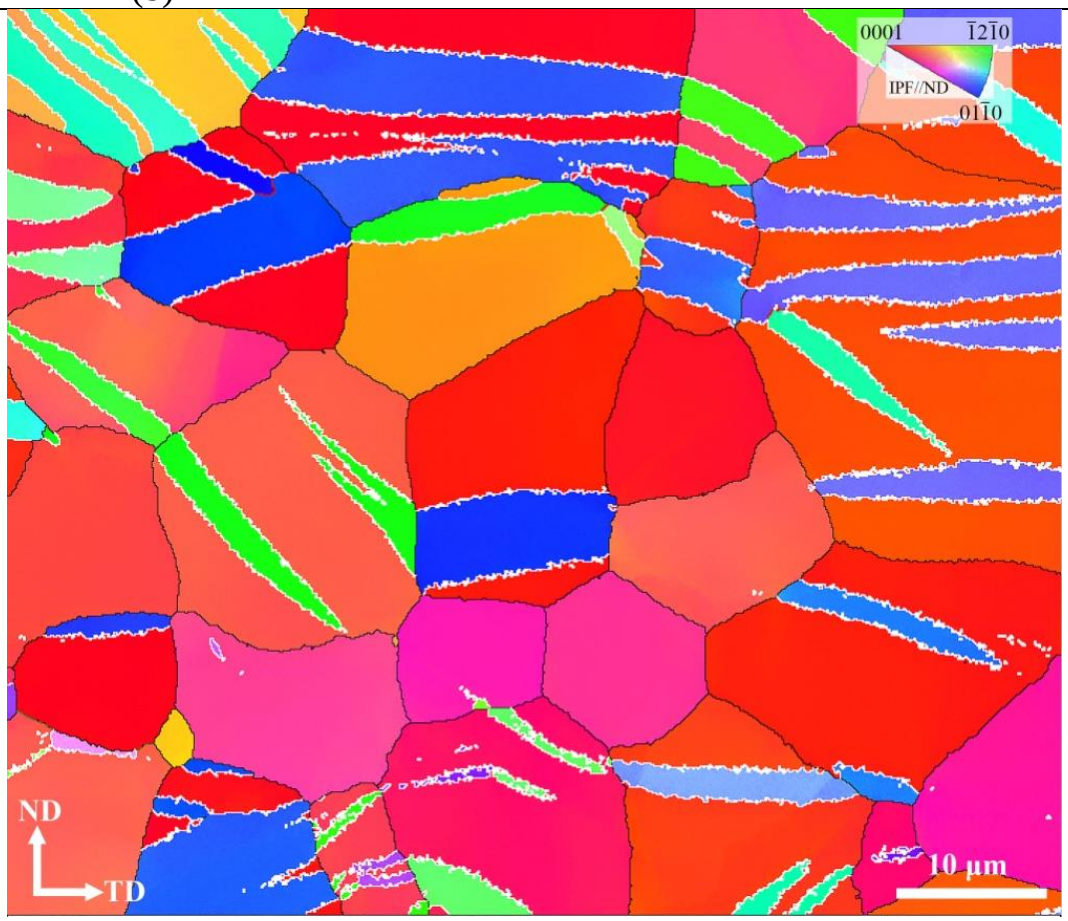

(c)

Fig. 1. (a) EBSD ND inverse pole figure micrograph of the initial material. (b) EBSD {0001} pole figure of the microstructure in (a). (c) A representative EBSD ND inverse pole figure micrograph of the deformed sample. Grain boundaries with a misorientation greater than 5° are outlined in black. {10−12} extension twins are outlined in white. Boundaries between different twin variants in a particular grain are outlined in red (not so frequent).

4. Classification of twin variants as a function of their stress free distortion

Since Schmid factor (SF) reflects how an individual twinning system activates, a grain-by-grain analysis of SF is conducted on 72 grains containing 176 ETWs. Fig. 2a shows cumulative frequency of twins in terms of their SFs. This presentation directly shows how often twins with SFs below a certain value appear. It is seen from Fig. 2a that the SFs of twins range from −0.08 to 0.5, indicating that even twins with very low SFs are initiated. A noticeable proportion (~22%) of twins have SFs lower than 0.25, which can be called as "low" SF twins. Furthermore, in order to know the preference of one twin in a particular grain, its SF rank [16] is determined through calculating SFs of all the six possible twin variants in the grain and then ranking the SFs decreasingly. Here, ranks "1" and "6" correspondto the highest and the lowest SF in one grain, respectively. Fig. 2b shows the frequency of the twins in terms of their SF ranks. It is seen that a noticeable proportion (~23%) of them falls into SF ranks “3” and “4”, though none falls into SF ranks “5” and “6”. In each rank, the SFs are dispersed in a wide range because of the variation of grain orientations. Therefore, even in SF ranks “1” and “2”, there are also low SF twins.

Further analysis is conducted to shed light on how the selection of twin variants is influenced by SF. Fig. 2c shows the frequency of grains containing various numbers of twin variants. It is seen that about 61% of the grains contain only one twin variant, while about 31% of them contain two twin variants. A few grains contain more than two twin variants. Fig. 2d shows the frequency of the twins in terms of their SF ranks as well as the number of twin variants in their associated grains. It is seen that, in grains containing only one twin variant, the majority of the twins are in SF ranks 1 and 2. However, in grains containing several twin variants, significantly more twins are in SF ranks 3 and 4. This indicates that the firstly formed twin variants have relatively high SF while the later formed ones have relatively low SFs. Comparing Fig. 2d with Fig. 2b, it can be found that, in grains containing 3 and 4 variants, SF ranges of ranks 1 and 2 are significantly narrowed into the sections of higher SFs. This indicates that the grains, which are more prone to be twinned, are likely to form multiple twin variants. Comparing Fig. 2d with Fig. 2a, it is found that the few cases of anomalous twins with negative SFs are in grains containing two twin variants, suggesting that their formation is probably due to complex stress conditions as a result of neighboring grains deformation and prior twinning.

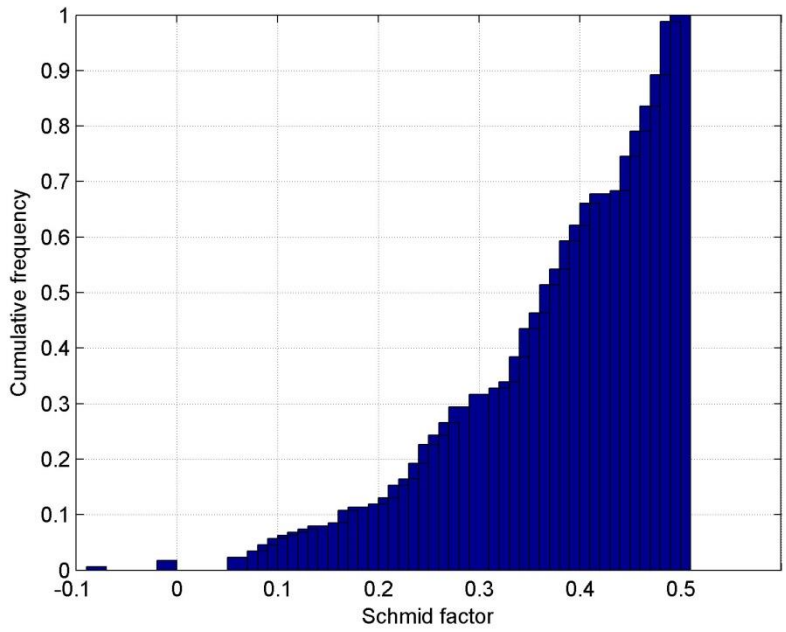
Cumulative frequency
Schmid factor
1
0.9
0.8
0.7
0.6
0.5
0.4
0.3
0.2
0.1
0
-0.1
0
0.1
0.2
0.3
0.4
0.5

(a)

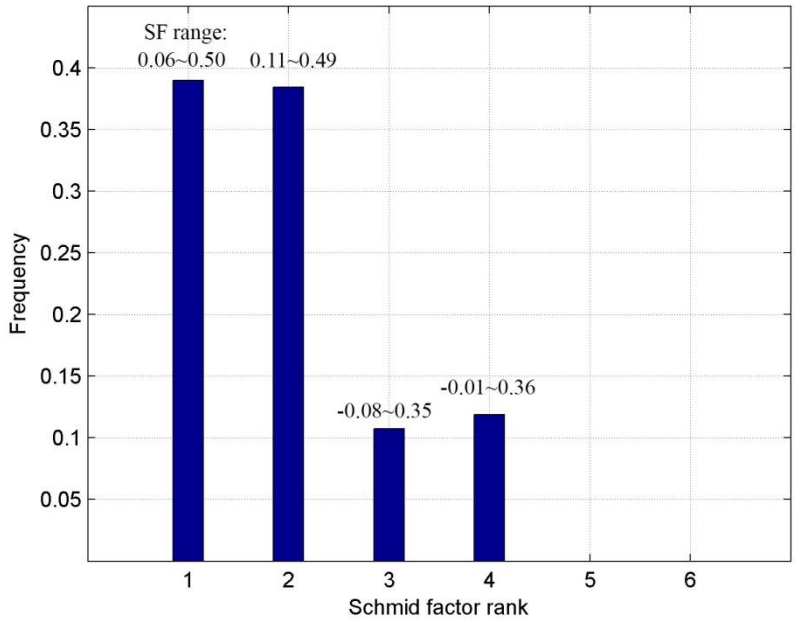
SF range:
0.06~0.50
0.11~0.49
-0.08~0.35
-0.01~0.36
Frequency
Schmid factor rank
0.4
0.35
0.3
0.25
0.2
0.15
0.1
0.05
1
2
3
4
5
6

(b)

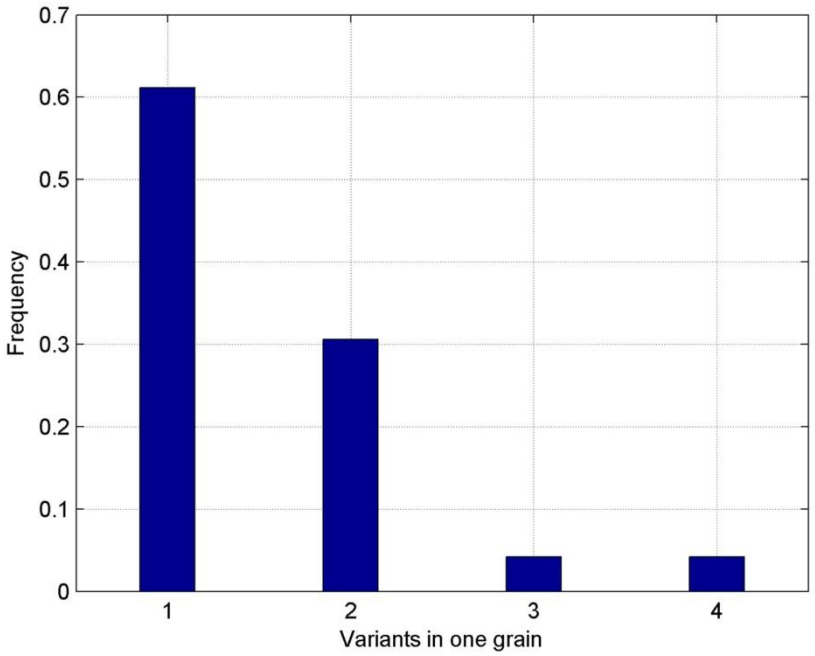

(c)

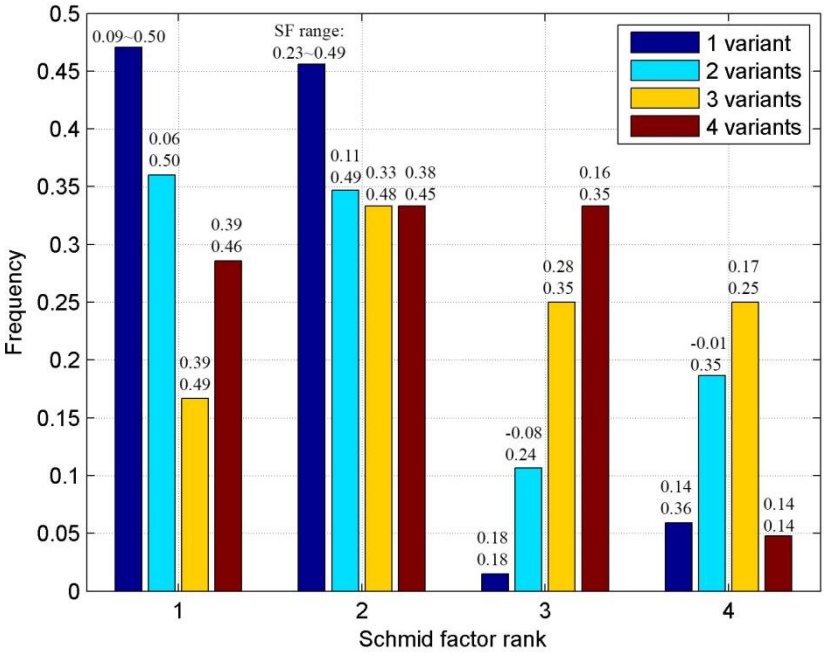

(d)

Fig. 2. (a) Cumulative frequency of SFs of the twins. (b) Frequency of the twins in terms of SF ranks (here, ranks “1” and “6” correspondto the highest and lowest SF in one grain, respectively). (c) Frequency of grains in terms of twin variants numbers. (d) Frequency of twins in terms of SF ranks as well as the number of twin variants in their associated grains (here, ranks “5” and “6” are omitted according to (b)).

The external strain conditions of the sample are $e_{RD} < 0$, $e_{TD} > 0$, and $e_{ND} > e_{TD} > 0$. Knowledge of the orientations of the grains, the twinning systems of the observed twin variants and the twinning shear enables the calculation of the displacement gradient (stress free distortion) tensor of a given twin in the sample coordinates (**x** // RD, **y** // TD and **z** // ND) using the simple Taylor assumption and disregarding elasticity, as presented in Appendix A. The diagonal components of such a tensor are e_{RD}, e_{TD} and e_{ND} of the twin. Fig. 3a shows the twins in e_{RD}-e_{ND} plane, in which four symbols denote the twins in the four quadrants, respectively. It can be seen that the majority of them lie in the second quadrant of $e_{RD} < 0$ and $e_{ND} > 0$, which agrees largely with the external strains. Guided by this figure, the twins are divided into four types as listed in Table 1. Since $e_{RD} + e_{TD} + e_{ND} = 0$ due to purely deviatoric twinning strain, some subgroups exist in Types B and D due to different signs of e_{TD}. Fig. 3b shows the twins in e_{TD}-e_{ND} plane with the symbols employed in Fig. 3a. It reveals that only a fraction of the twins, in the shaded area in Fig. 3b, approximately agree with the external strain boundary conditions.

It is insufficient to determine how the external boundary conditions influence the twinning types unless the orientations of the grains are taken into consideration. Therefore, the normal strain components of all six possible twin variants in a particular grain are calculated, and thus their types can be determined. Table 1 provides comprehensive comparisons between the observed twins (i.e., in "Exp" columns) and all possible twins (i.e., in "All" columns). It can be seen that the majority (~80%) of the observed twins belong to Type B, in which those with $e_{TD} > 0$ (subgroup B1) are approximately as many as those with $e_{TD} < 0$ (subgroup B2). This helps to understand why the specimen elongation along ND is larger than that along TD (cf. Section 3). Except Type A twin, the "Exp" frequencies of the other types are close to the "All" ones, which explains the absence of Type D2 twins. Since SF rank does not quantitatively give the relative magnitudes of SFs for a particular grain, SF ratio is defined as the ratio of the SF of a certain twin variant to the highest SF of the six possible twin variants in the same grain. Since the percentage of "SF ratio ≤ 0.50" is always lower than (or equal to) those of "SF ≤ 0.25" and "SF ranks 3 to 6" (Table 1), it is a more proper criterion for "low" SF twins. The majority (~91%) of the possible Type A twins are low SF twins whereas less than 50% of the other possible twin types are low SF twins. This explains the suppressed frequency of Type A twins. Comparing the "Exp" SF ratio with the "All" one, it can be seen that "high" SF twins (SF ratio > 0.5) in Types B and C with $e_{RD} < 0$ are strongly favored, but their occurrence in Types A and D

with $e_{RD} > 0$ is considerably weakened. The rare anomalous twins with SFs < 0 all belong to Types A and D.

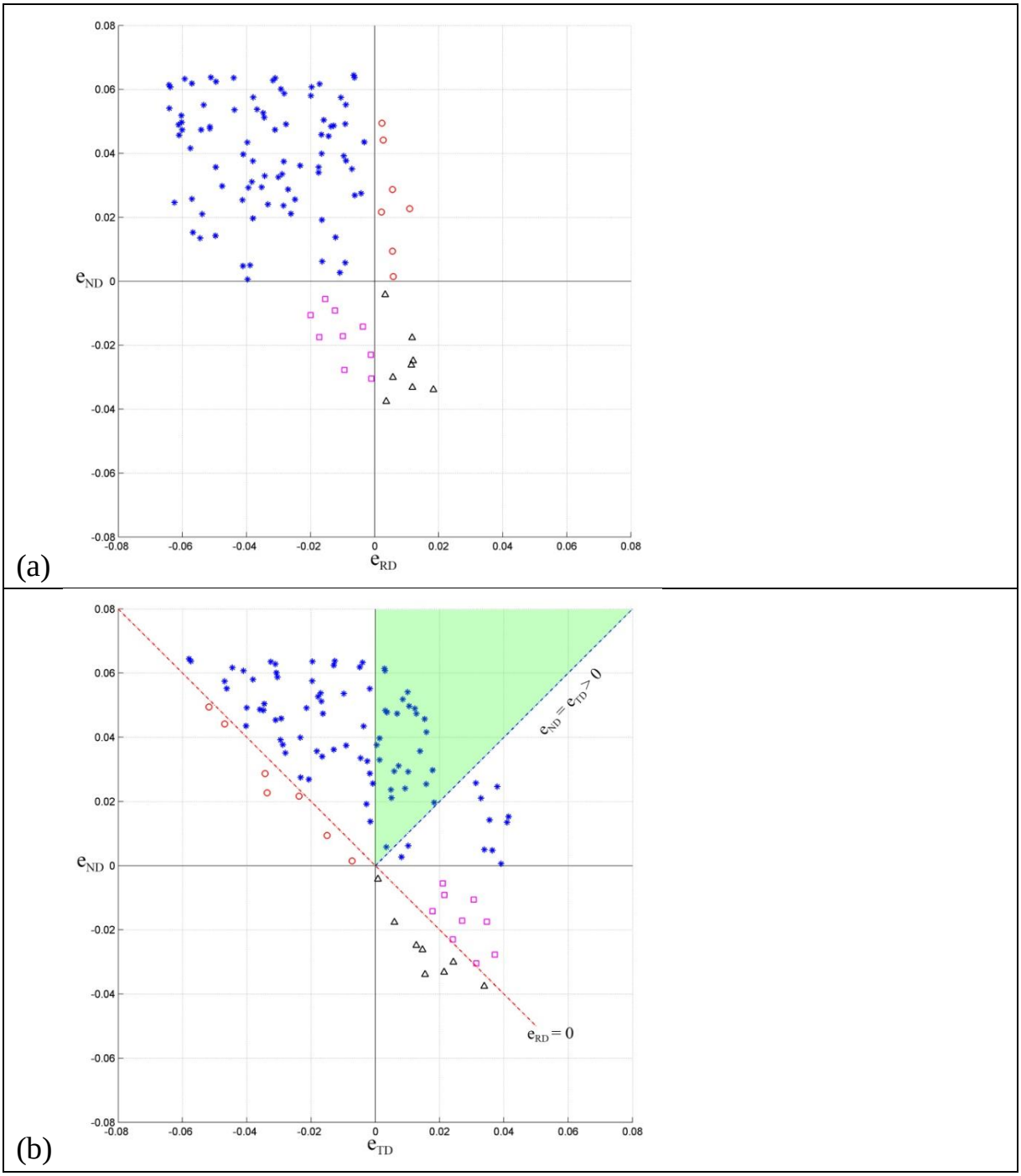

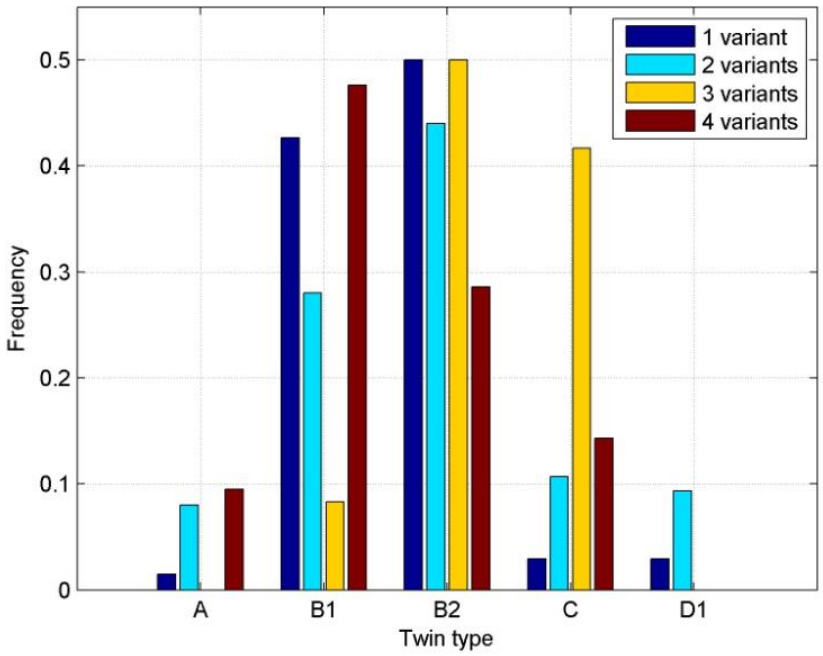

(c)

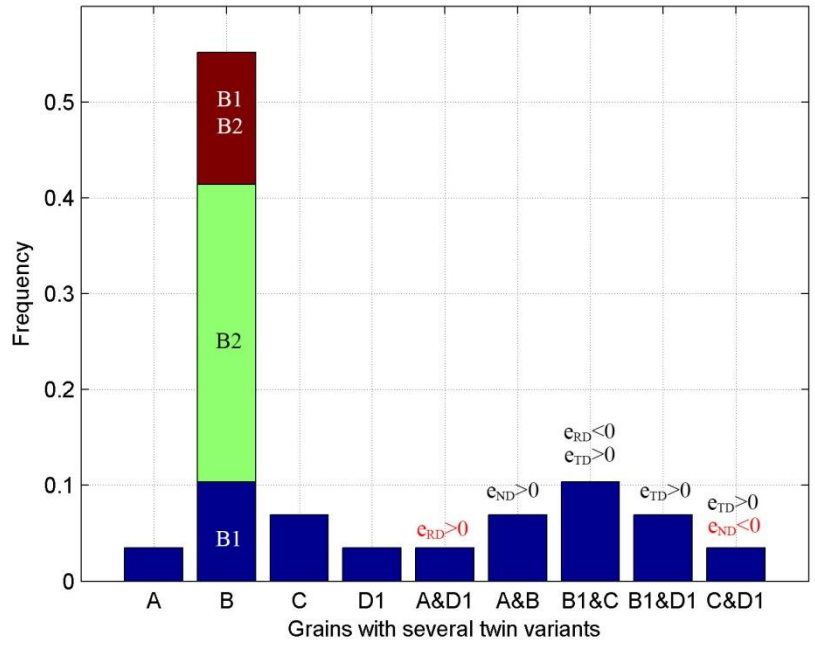

(d)

Fig. 3. Distribution of the twins in (a) e_{RD}-e_{ND} plane, and in (b) e_{TD}-e_{ND} plane. Since $e_{RD} + e_{TD} + e_{ND} = 0$, dashed lines in the (b) can be drawn. (c) Frequency of twins in terms of their types as well as the number of twin variants in their associated grains. (d) Frequency of grains with several twin variants in terms of twinning types.

Fig. 3c shows the frequency of twins in terms of their types as well as the numbers of twin variants in their associated grains. For the twinned grains containing only one twin variant, the majority (~93%) of the twins belong to Type

B. As co-existing twin variants form, the other types of twins increase. In spite of a variation of percentages of the twinning types for grains with several twin variants, the majority of them belong to Types B and C with $e_{RD} < 0$. This indicates that during deformation the preference of twinning types in a decreasing order is Type B, Type C, Types A and D, which agrees with their observed frequencies (Table 1). Fig. 3d shows the frequency of grains with several twin variants in terms of twinning types. It is seen that up to two twinning types may exist in one grain. The frequency of grains with Type B twin variants is significantly higher than the others. Among the three combinations of Type B subgroups, the frequency of grains with all twin variants of subgroup B2 is the highest. A significant proportion (~31%) of the grains has combined twinning types. Among these grains, those with twin types that deviate the most from the external strain conditions, i.e., Types "A & D1" and "C & D1", have a lower frequency. Moreover, Types "A & C" and "B2 & D1", composed of types with opposite signs for all the normal strain components, are absent.

Table 1. Characteristics of four types of twins, which are shown in Fig. 3.

Type (symbol)		e_{RD}	e_{TD}	e_{ND}	Frequency (%)		SF range		SF ≤ 0.25 (%)		SF ranks 3 & 4 (%)		SF ranks 5 & 6 (%)		SF ratio[3] ≤ 0.50 (%)	
					Exp[1]	All[2]	Exp	All	Exp	All	Exp	All	Exp	All	Exp	All
A (o)		+	–	+	5.11	13.19	–0.01 ~ 0.45	–0.22 ~ 0.45	66.67	94.49	44.44	26.32	None	63.16	44.44	91.23
B (*)	B1	–	+	+	34.66	31.71	0.09 ~ 0.50	–0.12 ~ 0.50	6.56	55.47	9.83	25.55	None	29.93	1.64	47.45
	B2	–	–	+	44.89	40.51	0.08 ~ 0.50	–0.05 ~ 0.50	17.72	62.29	13.92	34.29	None	26.86	5.06	49.14
C (□)		–	+	–	10.23	9.72	0.24 ~ 0.41	–0.16 ~ 0.41	33.33	57.14	72.22	38.10	None	45.24	0.00	47.62
D (Δ)	D1	+	+	–	5.11	4.40	–0.08 ~ 0.22	–0.08 ~ 0.30	100.00	84.21	77.78	73.68	None	5.26	22.22	42.11
	D2	+	–	–	0	0.46	None	–0.03 ~ 0.13	None	100.00	None	100.00	None	0.00	None	100.00

[1]Experimentally observed twins. [2]Take all the six possible twin variants in every twinned grain into consideration. [3]SF ratio is the ratio of the SF of a certain twin to the highest SF of the six possible twin variants in the same grain.

5. Mechanisms of low and even negative SF twin variants selection

5.1. Mechanism A: twin-to-twin strain accommodation

Figure 4a shows twins "1a and b" with negative SFs in grain "1". It can be seen that each twin is approximately in full contact with a high SF twin in the neighboring grains at the grain boundaries, i.e., twin "1a" with twin "2", and twin "1b" with twin "3". From the {0001} pole figure of the matrix of grain "1" and its six possible twin variants as shown in Fig. 4b, it is seen that twins "1a and b" correspond to the same variant, as enclosed by the circle in the figure. Firstly, the selection of twin "1a" rather than other twin variants with positive SFs is taken into consideration. As analyzed previously, the Type B twin "2" with a high SF probably forms earlier than the Type A twin "1a". Since the formation of twin "1a" requires shearing in the matrix, twin "2" in the neighborhood should accommodate the distortion induced by twin "1a". Accordingly, a quantitative method is next developed to calculate the components of the distortion in different deformation systems in twin "2".

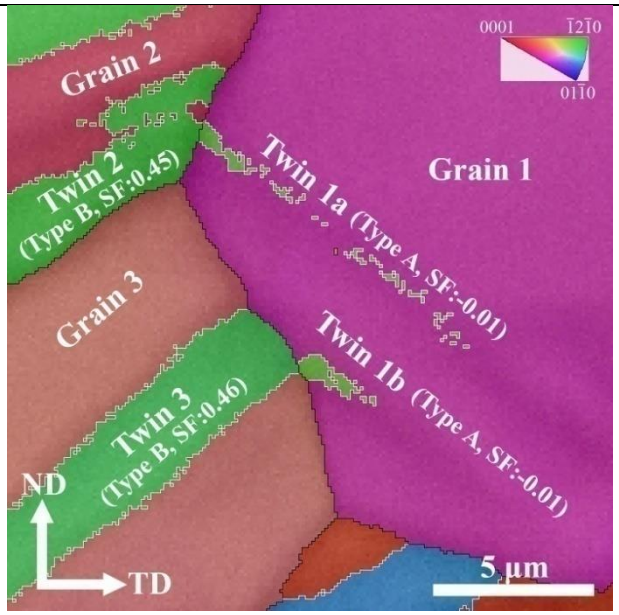

(a)

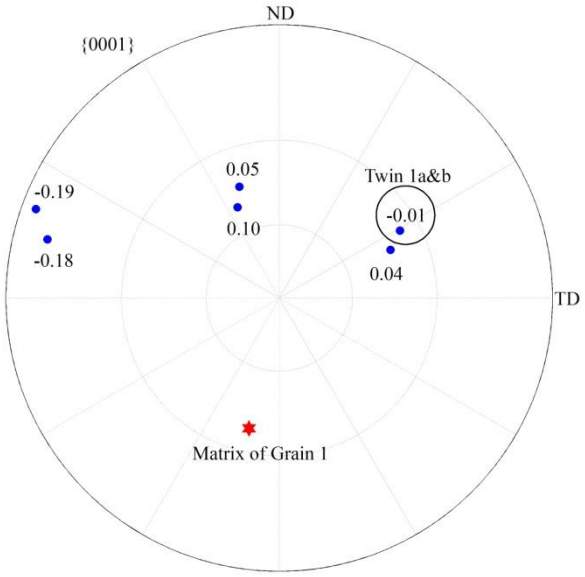
ND
{0001}
TD
0.05
0.10
-0.19
-0.18
Twin 1a&b
-0.01
0.04
Matrix of Grain 1

(b)

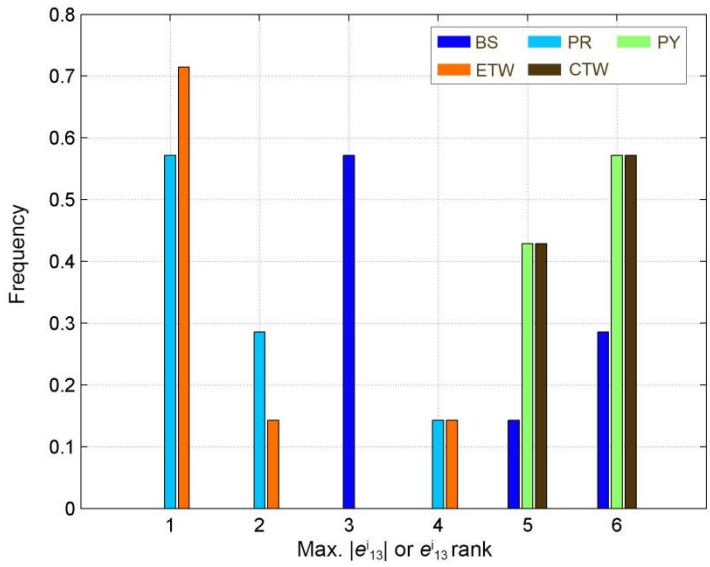
BS
PR
PY
ETW
CTW
Frequency
Max. |e^i_13| or e^i_13 rank

(c)

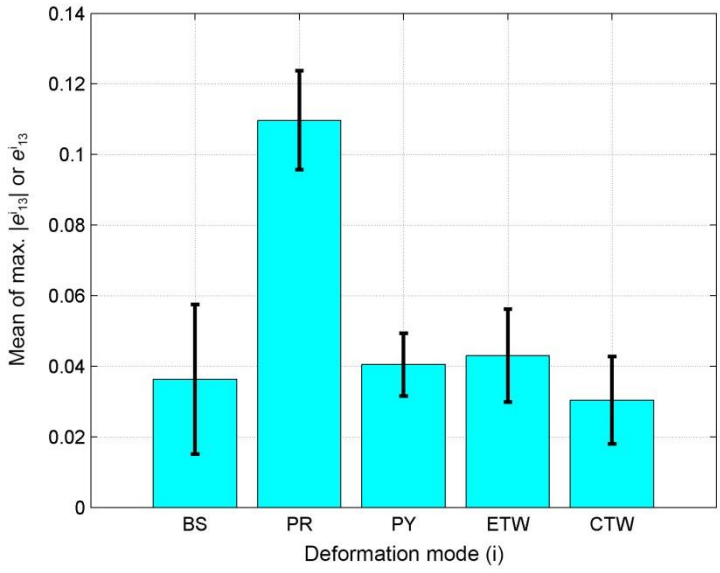
Mean of max. |e^i_13| or e^i_13
BS
PR
PY
ETW
CTW
Deformation mode (i)

(d)

Fig. 4. (a) EBSD ND inverse pole figure micrograph of twins with negative SFs and their surroundings. The same set of colored lines are employed as in Fig. 1c. (b) {0001} pole figure of the matrix of "grain 1" and its six possible twin variants with their SFs, in which the selected one is enclosed by a circle. (c) Frequency of low SF twins obeying "mechanism A", in terms of maximum $|e_{13}^{i}|$ or e_{13}^{i} rank (here, $|e_{13}^{i}|$ for slip systems, e_{13}^{i} for twinning systems, rank 1 to 6 in a decreasing sequence of $|e_{13}^{i}|$ or e_{13}^{i}). (d) Mean value of maximum $|e_{13}^{i}|$ or e_{13}^{i} of the selected twins for every deformation mode, with an error bar giving the standard deviation from the mean value.

The magnitude of twinning shear (γ) is 0.129 for {10−12} extension twin in Mg when the c/a ratio is 1.624. All the six possible twin variants in a particular grain have the same “displacement gradient tensor” introduced by [16] in their corresponding "natural" twinning basis, which is defined as $\mathbf{x_{ETW}}$ // shear direction, $\mathbf{y_{ETW}}$ // shear plane normal, and $\mathbf{z_{ETW}}$ // twinning plane normal, as listed in Table 2. It has a simple form:

$$E_{ij}^{ETW} = \begin{bmatrix} 0 & 0 & 0.129 \\ 0 & 0 & 0 \\ 0 & 0 & 0 \end{bmatrix}. \quad (1)$$

EBSD measured orientations of twinned-matrices and theoretical orientations of six possible twin variants in a particular grain are employed in the following analysis. The tensor E^{ETW} of each possible twin variant of grain "1" can be transformed in the orthonormal basis ($\mathbf{x}_{\mathbf{o}rt}$ // <10−10>, $\mathbf{y}_{\mathbf{o}rt}$ // <−12−10> and $\mathbf{z}_{\mathbf{o}rt}$ // <0001>) of twin "2" according to Appendix B, resulting in a total of six $E^{\mathbf{o}rt\text{-}T}$ matrices. Then, considering twin "2" as an individual grain, each $E^{\mathbf{o}rt\text{-}T}$ can be referred to the "natural" basis of a given slip or twinning system of twin "2". A logical continuation enables the definition of the "natural" basis of a twinning system according to the above $(\mathbf{x}\text{-}\mathbf{y}\text{-}\mathbf{z})_{\mathbf{ETW}}$ basis. However, for a slip system, its "natural" basis is constructed by **x** // slip direction, **z** // slip plane normal, and **y**-axis determined right-handedly. In the present paper, five common deformation modes are taken into consideration. The "natural" axes of these deformation systems are also listed in Table 2.

The general form of any $E^{\mathbf{o}rt\text{-}T}$ in the "natural" basis of a given deformation (slip or twinning) mode “i” is:

$$E_{ij}^{i} = \begin{bmatrix} e_{11}^{i} & e_{12}^{i} & e_{13}^{i} \\ e_{21}^{i} & e_{22}^{i} & e_{23}^{i} \\ e_{31}^{i} & e_{32}^{i} & e_{33}^{i} \end{bmatrix}. \quad (2)$$

The abbreviated names of the different deformation modes (BS for basal slip, etc) are given in Table 2. According to the physical meanings associated with the components of the "displacement gradient tensor" [16], e_{13}^{i} in the E^{i} matrix corresponds to the shear required to be accommodated by this deformation mode. The calculation method for E^{i} is also provided in Appendix B. These calculations lead to 24 values of e_{13}^{i} for one possible twin variant in grain "1", which equals to the numbers of all the variants of the deformation systems listed in Table 2. Therefore, there are 144 values of e_{13}^{i} for all the six possible twin variants in grain "1".

Table 2. The natural axes and numbers of variants of five common deformation modes in Mg alloys.

Systems (i)	Basal slip (BS)	Prismatic Slip (PR)	Pyramidal Slip (PY)	{10–12} extension twinning (ETW)	{10–11} contraction twinning (CTW)
variant	3	3	6	6	6
x-axis //	<–12–10>	<–12–10>	<2–1–1–3>	<–1011>	<10–1–2>
y-axis //	<–1010>	<0001>	<01–10>	<–12–10>	<–12–10>
z-axis[1] //	<0001>	<10–10>	<14–7–78>	<80–89>	<70–74>

[1]More accurate z-axis of PY, ETW and CTW is <14.06, –7.03, –7.03, 8>, <7.91, 0, –7.91, 9>, and <7.03, 0, –7.03, 4>, respectively.

Among the five deformation modes, basal slip (BS) can be activated most easily due to its relatively low CRSS. Comparatively, the CRSS of prismatic slip (denoted PR in Table 2) in AZ31 alloy is 1.1 to 5.5 times of that of BS [2, 20]. Although the pyramidal <c+a> slip (PY) with a significantly higher CRSS [20] may occur, its contribution has been reported to be very small [21]. As to twinning, {10–12} extension twinning (ETW) has a low CRSS about 2 times of that of BS [1], while {10–11} contraction twinning (CTW) has a significantly higher CRSS comparable to that of PY [2]. Table 3 lists the maximum absolute values of e_{13}^{i} for each slip system and the maximum values of e_{13}^{i} for each twinning system associated with the six possible twin variants in grain "1", which contains a total of 30 values. It can be seen that the selected twin "1a" has the lowest $|e_{13}^{PY}|$ and e_{13}^{CTW}, but the highest $|e_{13}^{PR}|$ and e_{13}^{ETW}.

About 64% of the low SF twins including all the negative SF ones can be explained by this mechanism, while the rest of them will be explained in the next

section. Fig. 4c shows the frequency of the twins obeying mechanism A in terms of the maximum $|e_{13}^{i}|$ or e_{13}^{i} rank. It can be seen that all of the selected twins have low $|e_{13}^{PY}|$ and e_{13}^{CTW} in ranks 5 and 6, while the majority (> 80%) of them have high $|e_{13}^{PR}|$ and e_{13}^{ETW} in ranks 1 and 2. It reveals that the accommodation of twinning variants with low or even negative SF is mostly carried out by deformation systems with low CRSSs. Fig. 4d shows the mean value of the maximum $|e_{13}^{i}|$ or e_{13}^{i} of the selected low SF twins for every deformation mode. It can be seen that the mean value of $|e_{13}^{PR}|$ (i.e. prismatic slip) is considerably larger than the others. This indicates that the activity of prismatic slip is more enhanced by interfacial strain compatibility, which agrees with Ref. [22].

Table 3. The Schmid factors, the maximum $|e_{13}^{i}|$ (for slip modes) and e_{13}^{i} (for twinning modes) in "twin 2", which are induced by the six possible twin variants in "grain 1", respectively (Fig. 4a). The values in the row of "twin 1a" is highlighted.

Variant	SF	$\lvert e_{13}^{BS}\rvert$	$\lvert e_{13}^{PR}\rvert$	$\lvert e_{13}^{PY}\rvert$	e_{13}^{ETW}	e_{13}^{CTW}
1	–0.19	0.0310	0.0484	0.1199	0.0105	0.1152
2	0.05	0.0302	0.0840	0.1006	0.0186	0.0872
3	**–0.01**	**0.0372**	**0.1208**	**0.0302**	**0.0477**	**0.0235**
4	–0.18	0.0818	0.0517	0.1000	0.0105	0.0817
5	0.10	0.0733	0.0698	0.0800	0.0185	0.0720
6	0.04	0.0058	0.1115	0.0428	0.0472	0.0410

5.2 Mechanism B: twin-to-grain strain accommodation

Fig. 5a shows a low SF twin in grain "4" and its neighborhood. It can be seen that twin "4a" has a high SF while twin "4b" has a much lower SF. Fig. 5b shows the {0001} pole figure of the twinned-matrix of grain "4" and its six possible twin variants. Except twin "4a", there are other possible twin variants with SFs higher than that of twin "4b". However, they are absent. Since twin "4b" adjoins the twinned-matrix of grain "5", E^{ETW} of each possible twin variant in grain "4" is transformed to the orthonormal basis of the twinned-matrix of grain "5", which is different from the analysis of twin "1a" in Fig. 4a. The resulted matrix is designated as $E^{ort\text{-}M}$, the calculation method of which is also provided in Appendix B. Then, E^{i} corresponding to $E^{ort\text{-}M}$ can be calculated. Table 4 lists the maximum $|e_{13}^{i}|$ or e_{13}^{i} in the same manner as Table 3. It can be seen that the

selected twin "4b" has the lowest $|e_{13}^{PY}|$, but the highest $|e_{13}^{BS}|$. Fig. 5c shows the frequency of low SF twins obeying this mechanism in terms of the maximum $|e_{13}^{i}|$ or e_{13}^{i} rank. It reveals that all of them have low $|e_{13}^{PY}|$ in ranks 5 and 6, but high $|e_{13}^{BS}|$ in ranks 1 and 2. Besides, the majority (>70%) of them have low e_{13}^{CTW} in ranks 5 and 6. Fig. 5d shows the mean value of the maximum $|e_{13}^{i}|$ or e_{13}^{i} of the selected low SF twins for every deformation mode. It can be seen that the mean value of $|e_{13}^{BS}|$ is noticeably larger than the others, indicating that the shear induced by a low SF twin is mainly accommodated through basal slip in its neighboring grain. By now, the selection of all the low SF twins (Table 1) has been interpreted.

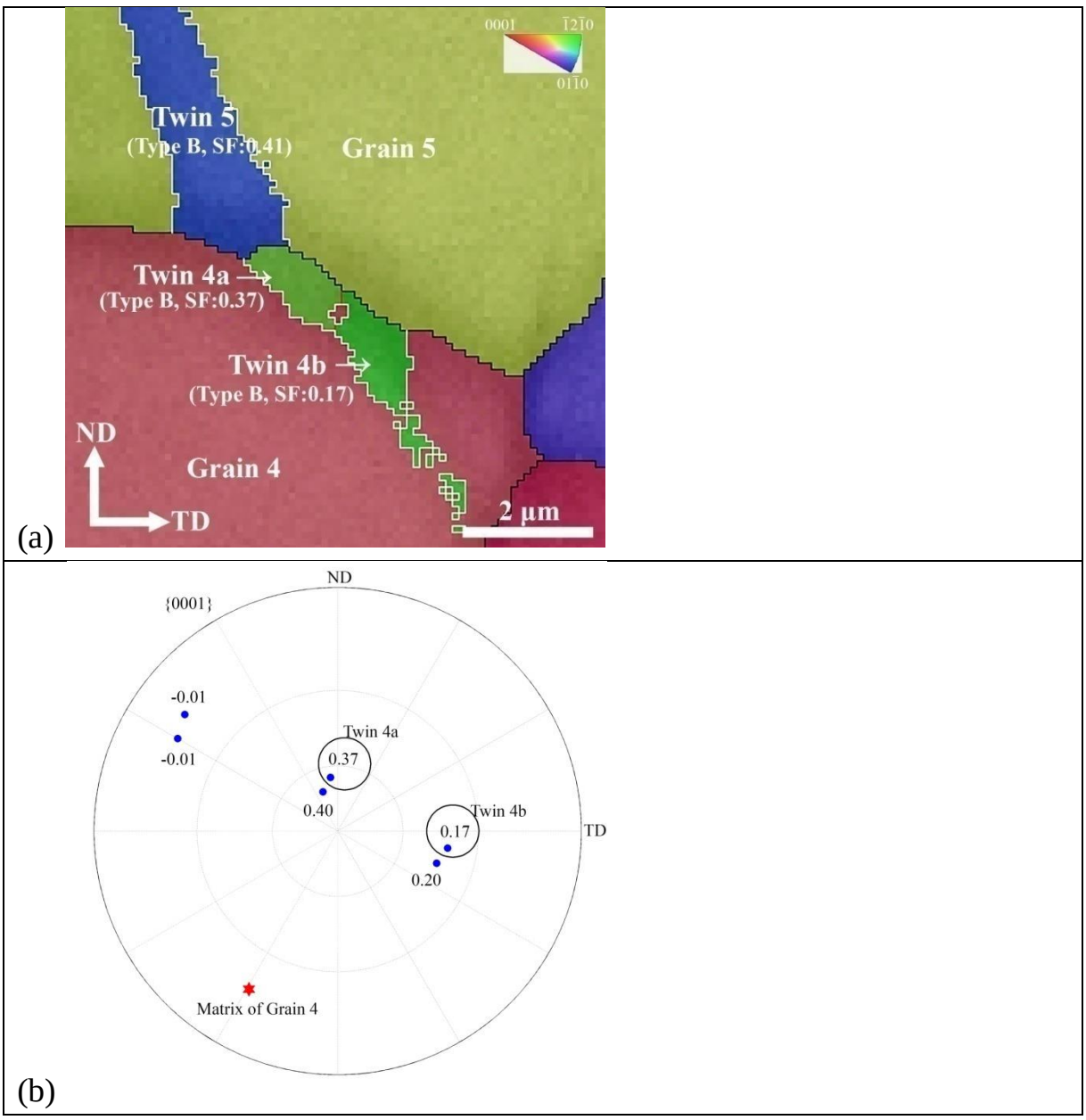

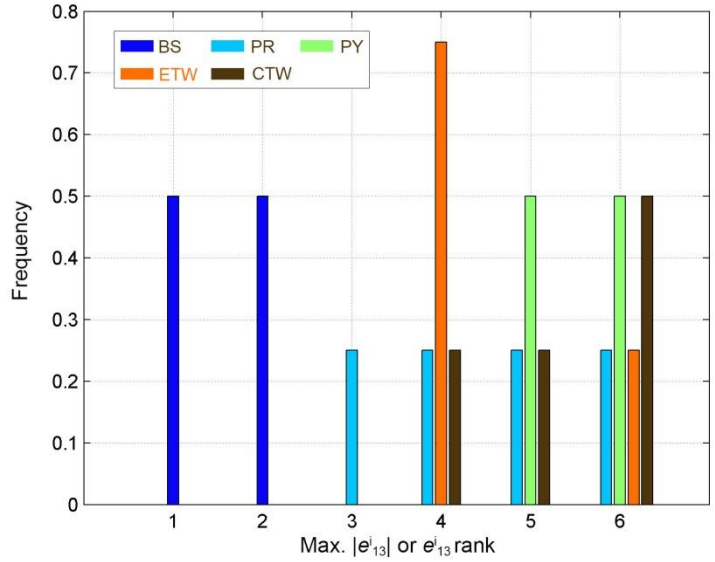

(c)

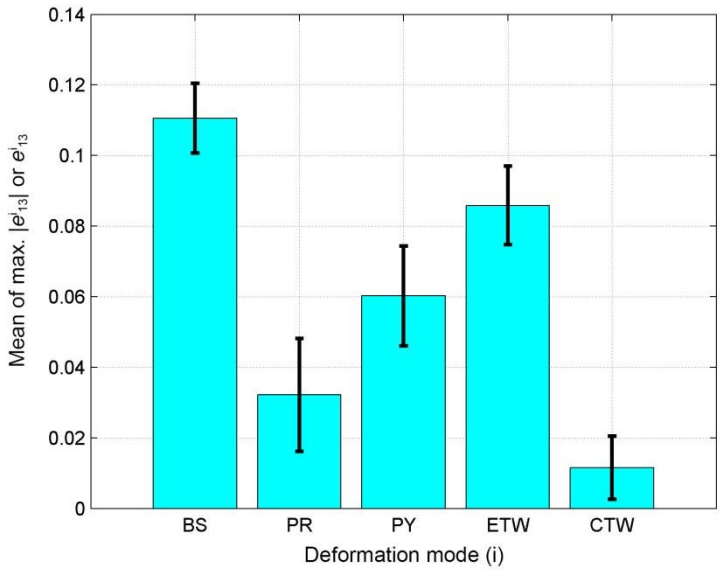

(d)

Fig. 5. (a) EBSD ND inverse pole figure micrograph of a low SF twin and its surrounding. The same set of colored lines are employed as in Fig. 1c. (b) {0001} pole figure of the matrix and twins in grain 4 in the style of (a). (c) Frequency of low SF twins governed by "mechanism B", in terms of maximum $|e_{13}^i|$ or e_{13}^i rank (in the same style of Fig. 4c). (d) Mean value of maximum $|e_{13}^i|$ or e_{13}^i of the selected twins for every deformation mode, with an error bar giving the standard deviation from the mean value.

Table 4. The Schmid factors, the maximum $|e_{13}^i|$ (for slips) and e_{13}^i (for twinnings) in "grain 5", which are induced by the six possible twin variants in "grain 4", respectively (Fig. 5a). The values in the row of "twin 4b" is highlighted.

Variant	SF	$\lvert e_{13}^{BS} \rvert$	$\lvert e_{13}^{PR} \rvert$	$\lvert e_{13}^{PY} \rvert$	e_{13}^{ETW}	e_{13}^{CTW}
1	–0.01	0.0178	0.0442	0.1204	0.0894	0.0542
2	0.37	0.0644	0.0632	0.1024	0.0972	0.0123
3	**0.17**	**0.1159**	**0.0249**	**0.0694**	**0.0902**	**0.0069**
4	–0.01	0.1110	0.0319	0.0730	0.0893	0.0059
5	0.40	0.0550	0.0673	0.1072	0.0971	0.0182
6	0.20	0.0147	0.0380	0.1208	0.0903	0.0558

5.3 Rules underlying the two mechanisms

It is essentially consistent that both mechanisms favor twin variants that induce the least shear onto the deformation modes with high CRSSs (i.e., PY or CTW), but the most shear onto those with low CRSSs (i.e., BS, PR or ETW), in their neighboring "strain receiver" (i.e., twins for "mechanism A" while grains for "mechanism B"). However, strain applicators (i.e., the low SF twins) required major accommodation through PR for "mechanism A", while through BS for "mechanism B".

Fig. 6a shows the mean value of the maximum |SFs| (for slip) or SFs (for twinning) for every deformation mode of the grains containing the strain applicators and that of the strain receivers in condition of "mechanism A". It can be seen that the grain of strain applicator has high SF for ETW and low SF for CTW, while the strain receiver is in the opposite situation due to the external stress. Among the remainder deformation modes, the $|SF_{PR}|$ (i.e., |SF| for PR) difference of the counterparts is considerably larger than the others. The grain of strain applicator has a higher $|SF_{PR}|$. This indicates that a low SF twin under "mechanism A" forms in the grain where prismatic slip is more active. There exists a gradient of prismatic slip activity (i.e., PR gradient) across the boundary where the twin nucleates. Combining Fig. 4 together with Fig. 6a, it can be deduced that the selected low SF twins under "mechanism A" tend to flatten the PR gradient. Fig. 5b shows the data of "mechanism B" analogous to that of Fig. 5a. Conversely, it is $|SF_{BS}|$ rather than $|SF_{PR}|$ difference which is prominent. The grain of strain applicator has a higher $|SF_{BS}|$, indicating that a low SF twin under "mechanism B" forms in the grain where basal slip is more active. There exists a gradient of basal slip activity (i.e., BS gradient) across the boundary where the twin nucleates. Combining Fig. 5 together with Fig. 6b, it can be deduced that the selected low SF twins under "mechanism B" tend to flatten the BS gradient. Therefore, it is also essentially consistent that a low SF twin, under both mechanisms, tends to

flatten the slip gradient across the boundary where twinning nucleates for a certain slip mode with a low CRSS (PR or BS) . Such configurations contribute to local strain compatibility during plastic deformation.

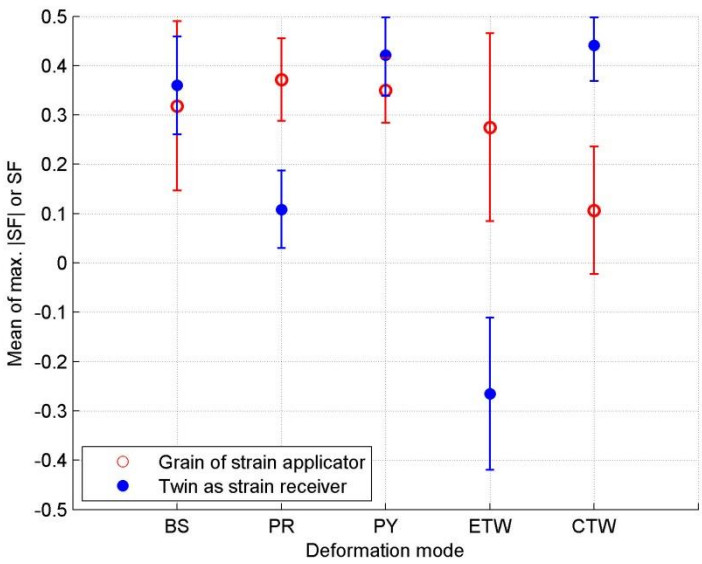

(a)

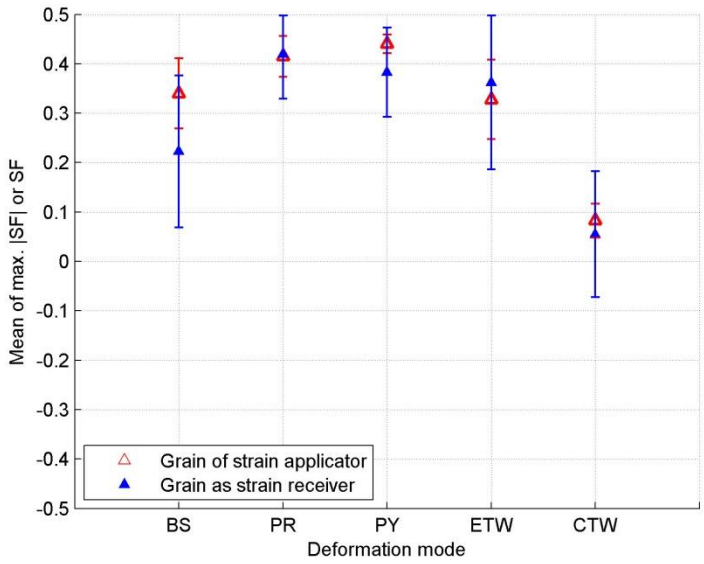

(b)

Fig. 6. Mean of maximum |SFs| or SFs (the former for slip systems while the latter for twinning systems) of grains containing low SF twins (i.e., grains of strain applicators) and (a) of neighboring high SF twins as strain receivers (Mechanism A), and of (b) neighboring grains as strain receivers (Mechanism B). Error bars give the standard deviations from the mean values.

6. Conclusions

{10−12} extension twinning during uniaxial compression of a typical basal textured AZ31 plate has been investigated. Special attention is paid to the relationship between the twin shear and the applied strains, and the selection of "low Schmid factor" twins. The analyses of the microstructure based on EBSD measurements and on twinning stress free distortion tensor transformation rules lead to the following conclusions.

1. Four types of twins are classified according to their stress free strains expressed along the global RD, TD, and ND directions of the sample. The frequency of "Type B" twins with $e_{RD} < 0$ and $e_{ND} > 0$, which is more adapted with the applied strains (i.e., $e_{RD} < 0$, $e_{TD} > 0$, $e_{ND} > e_{TD} > 0$), is considerably higher than the others. "Types A and D" twins with $e_{RD} > 0$ are suppressed, since they exerted elongation strains along RD, which conflicts with the RD compression loading of the sample.

2. A proportion of the twinned grains contains several twin variants up to 4. The frequency of "Type B" twins in grains containing only one variant is predominantly high, indicating that this type of twins firstly forms during the deformation. Most of them have relatively high Schmid factors (i.e., SF ratios > 0.5). In the grains containing several variants, the frequencies of other types of twins increase, among which that of "Type C" with $e_{RD} < 0$ increases the most. All of the "Type C" twins have relatively high SFs. The majority of the low SF twins (i.e., SF ratios ≤ 0.5) are "Types A and D" twins. It indicates that "Types B and C" twins, which formed earlier during the deformation, are initiated mainly by the external stress. However, noticeable proportion of "Types A and D" twins are initiated by the requirement of local strain compatibility.

3. Based on the concept of “displacement gradient tensor” introduced by Jonas et al. [16], a method is developed to calculate the tensor E^{ETW}, describing the twinning shear of a twin, in the "natural bases" of the deformation systems (three slip modes and two twinning modes) of a high SF twin or the matrix in its neighboring grain, resulting in tensor E^i. The "natural basis" of a slip (or twinning) system is defined as **x** // slip (or twinning shear) direction, **z** // slip (or twinning habit) plane normal and **y** is determined right-handedly. Only component e_{13}^i of the tensor E^i has a physical meaning, which is the distortion required to be accommodated by a deformation system.

4. Guided by the calculation method above, two mechanisms of low SF twin selection have been revealed. The physical basis of both the mechanisms is that the shear of a low SF twin (i.e., strain applicator) should be accommodated

by a twin or the matrix (i.e., strain receiver) in its neighboring grain, which connects the low SF twin at the grain boundary. The strain receiver is a high SF twin in mechanism A, while it is a twinned-matrix in mechanism B. For a grain containing a low SF twin, $|e_{13}^{i}|$ (for slip modes) or e_{13}^{i} (for twinning modes) components of five deformation systems associated with all the six possible twin variants in this grain are calculated. $|e_{13}^{BS}|$, $|e_{13}^{PR}|$, and e_{13}^{ETW} are associated with deformation systems with low CRSSs, while $|e_{13}^{PY}|$ and e_{13}^{CTW} are associated with those with high CRSSs. Their maximum values reveal a trend. All the selected twins have relatively low $|e_{13}^{PY}|$, but relatively high $|e_{13}^{PR}|$ in mechanism A while $|e_{13}^{BS}|$ in mechanism B. This difference is due to the difference of prismatic slip (PR) activity in mechanism A while that of basal slip (BS) activity in mechanism B between the grain of strain applicator and the strain receiver. The formation of the low SF twins contributes to the local strain compatibility.

Acknowledgements

The authors acknowledge the support of the French National Research Agency under the project MAGTWIN (referenced as ANR-12-BS09-0010-02)

Appendix A

A.1 Calculating e_{RD}, e_{TD} and e_{ND} for a twin

The lattice parameters of Mg are a = 0.3209 nm and c = 0.5211 nm (c/a = 1.624). The crystallographic basis $(\mathbf{x}\text{-}\mathbf{y}\text{-}\mathbf{z})_{\mathbf{cry}}$ of Mg is defined as $\mathbf{x}_{\mathbf{cry}}$ // <2−1−10>, $\mathbf{y}_{\mathbf{cry}}$ // <−12−10> and $\mathbf{z}_{\mathbf{cry}}$ // <0001>. The orthonormal basis $(\mathbf{x}\text{-}\mathbf{y}\text{-}\mathbf{z})_{\mathbf{ort}}$ of any twinned-matrix or twin is defined as $\mathbf{x}_{\mathbf{ort}}$ // <10−10>, $\mathbf{y}_{\mathbf{ort}}$ // <−12−10> and $\mathbf{z}_{\mathbf{ort}}$ // <0001>. The matrix "A" transform a vector in real space from basis $(\mathbf{x}\text{-}\mathbf{y}\text{-}\mathbf{z})_{\mathbf{cry}}$ to basis $(\mathbf{x}\text{-}\mathbf{y}\text{-}\mathbf{z})_{\mathbf{ort}}$ is:

$$A = \begin{bmatrix} \sqrt{3}a/2 & 0 & 0 \\ -a/2 & a & 0 \\ 0 & 0 & c \end{bmatrix}. \quad \text{(A1)}$$

While the matrix "A*" transform a vector in reciprocal space from basis $(\mathbf{x}\text{-}\mathbf{y}\text{-}\mathbf{z})_{\mathbf{cry}}$ to basis $(\mathbf{x}\text{-}\mathbf{y}\text{-}\mathbf{z})_{\mathbf{ort}}$ is:

$$A^* = (A^{-1})'. \quad \text{(A2)}$$

Using matrices "A and A*", the coordinates of any direction and plane normal of Mg crystal in the orthonormal basis can be determined.

For every possible twin variant in a grain, the displacement gradient tensor E^{ETW} in its "natural" twinning basis $(\mathbf{x}\text{-}\mathbf{y}\text{-}\mathbf{z})_{\mathbf{ETW}}$ (Table 2) is provided by Eq.(1) in the manuscript. The matrix transforms basis $(\mathbf{x}\text{-}\mathbf{y}\text{-}\mathbf{z})_{\mathbf{ETW}}$ to basis $(\mathbf{x}\text{-}\mathbf{y}\text{-}\mathbf{z})_{\mathbf{ort}}$ is:

$$R_1 = A \cdot [\mathbf{x}_{\mathbf{ETW}}, \mathbf{y}_{\mathbf{ETW}}, \mathbf{z}_{\mathbf{ETW}}], \quad \text{(A3)}$$

where $\mathbf{x}_{\mathbf{ETW}}$, $\mathbf{y}_{\mathbf{ETW}}$, and $\mathbf{z}_{\mathbf{ETW}}$ are column vectors. The map basis $(\mathbf{x}\text{-}\mathbf{y}\text{-}\mathbf{z})_{\mathbf{map}}$ of EBSD measurements on the deformed microstructure in this paper is defined as $\mathbf{x}_{\mathbf{map}}$ // TD, $\mathbf{y}_{\mathbf{map}}$ // ND and $\mathbf{z}_{\mathbf{map}}$ // RD. Using the measured Euler angles of a twinned-matrix, the matrix "R_2" rotating basis $(\mathbf{x}\text{-}\mathbf{y}\text{-}\mathbf{z})_{\mathbf{ort}}$ to basis $(\mathbf{x}\text{-}\mathbf{y}\text{-}\mathbf{z})_{\mathbf{map}}$ can be determined [23]. The sample basis $(\mathbf{x}\text{-}\mathbf{y}\text{-}\mathbf{z})_{\mathbf{sp}}$ of the specimen is defined as $\mathbf{x}_{\mathbf{sp}}$ // RD, $\mathbf{y}_{\mathbf{sp}}$ // TD and $\mathbf{z}_{\mathbf{sp}}$ // ND. The matrix rotating basis $(\mathbf{x}\text{-}\mathbf{y}\text{-}\mathbf{z})_{\mathbf{map}}$ to basis $(\mathbf{x}\text{-}\mathbf{y}\text{-}\mathbf{z})_{\mathbf{sp}}$ is:

$$R_3 = \begin{bmatrix} 0 & 0 & 1 \\ 1 & 0 & 0 \\ 0 & 1 & 0 \end{bmatrix}. \quad \text{(A4)}$$

Therefore, the equation transforming E^{ETW} in basis $(\mathbf{x}\text{-}\mathbf{y}\text{-}\mathbf{z})_{\mathbf{ETW}}$ to basis $(\mathbf{x}\text{-}\mathbf{y}\text{-}\mathbf{z})_{\mathbf{sp}}$ is:

$$E^{sp} = R_4 \cdot E^{ETW} \cdot R_4^{-1} = \begin{bmatrix} e_{RD} & e_{12} & e_{13} \\ e_{21} & e_{TD} & e_{23} \\ e_{31} & e_{32} & e_{ND} \end{bmatrix}, \quad \text{(A5)}$$

where $R_4 = R_3 \cdot R_2 \cdot R_1$.

Appendix B

B.1 Calculation of $E^{ort\text{-}M}$ and $E^{ort\text{-}T}$

According to the definition of R_2 in Appendix A, the matrix that transforms the orientation of the twinned-matrix in "grain 1" to that of the twinned-matrix in "grain 2" (Fig. 4a) is:

$$R_5 = (R_2^{g2})^{-1} \cdot R_2^{g1}, \quad \text{(B1)}$$

where the superscript "g1" and "g2" refers to "grain 1" and "grain 2", respectively. The equation that transforms E^{ETW} from basis $(\mathbf{x}\text{-}\mathbf{y}\text{-}\mathbf{z})_{\mathbf{ETW}}$ in "grain 1" to basis $(\mathbf{x}\text{-}\mathbf{y}\text{-}\mathbf{z})_{\mathbf{ort}}$ in "grain 2" is:

$$E^{ort\text{-}M} = R_6 \cdot E^{ETW} \cdot R_6^{-1}, \quad \text{(B2)}$$

where $R_6 = R_5 \cdot R_1$.

In "grain 2" (Fig. 4a), the matrix R_7 that rotates basis $(\mathbf{x}\text{-}\mathbf{y}\text{-}\mathbf{z})_{\mathbf{ort}}$ of the twinned-matrix to that of the "twin 2" can be easily determined according to twinning geometry. Then, the matrix $E^{ort\text{-}T}$ can be calculated by:

$$E^{ort\text{-}T} = R_7 \cdot E^{ort\text{-}M} \cdot R_7^{-1}. \quad \text{(B2)}$$

B.2 Calculation of E^{i}

The matrix that transforms the basis $(\mathbf{x}\text{-}\mathbf{y}\text{-}\mathbf{z})_{ort}$ of "twin 2" to the natural basis $(\mathbf{x}\text{-}\mathbf{y}\text{-}\mathbf{z})_{i}$ of any of the five deformation systems in Table 2 is:

$$R_8 = (A \cdot [\mathbf{x_i}, \mathbf{y_i}, \mathbf{z_i}])^{-1}. \quad \text{(B3)}$$

Then, the matrix E^{i} can be calculated by:

$$E^{i} = R_8 \cdot E^{ort} \cdot R_8^{-1}. \quad \text{(B4)}$$

References

[1] S.R. Agnew, Ozgür Duygulu, International Journal of Plasticity 21 (2005) 1161–1193.

[2] J. Koike, Metall. Mater. Trans. A 36 (2005) 1689–1696.

[3] M.R. Barnett, Mat. Sci. Eng. A 464 (2007) 1-7.

[4] M.R. Barnett, Z. Keshavarz, A.G. Beer and D. Atwell, Acta Mater. 52 (2004) 5093–5103.

[5] L. Jiang, J. J. Jonas, A. Luo, A.K. Sachdev and S. Godet, Scr. Mater. 54 (2006) 771–775.

[6] M.D. Nave, M.R. Barnett, Scr. Mater. 51 (2004) 881–885.

[7] P. Yang, Y. Yu, L. Chen and W. Mao, Scr. Mater. 50 (2004) 1163–1168.

[8] S. Godet, L. Jiang, A.A. Luo and J.J. Jonas: Scr. Mater. 55 (2006) 1055–1058.

[9] L. Jiang, J.J. Jonas, R.K. Mishra, A.A. Luo, A.K. Sachdev and S. Godet, Acta Mater. 55 (2007) 3899–38910.

[10] D.W. Brown, S.R. Agnew, M.A.M. Bourke, T.M. Holden, S.C. Vogel, C.N. Tome, Mat. Sci. Eng. A 399 (2005) 1–12.

[11] M. Gharghouri, G. Weatherly, J. Embury, J. Root, Phil. Mag. A 79 (7) (1999) 1671–1695.

[12] J. Koike, Y. Sato and D. Ando, Materials Transactions, 49(12) (2008) 2792–2800.

[13] A. Jain, O. Duygulu, D.W. Brown, C.N. Tome and S.R. Agnew, Mater. Sci. Eng. A 486 (2008) 545–555.

[14] M.R. Barnett, Z. Kechavarz and M.D. Nave, Metall. Mater. Trans. A 36A (2005) 1697–1704.

[15] L. Jiang, A. Godfrey, W. Liu and Q. Liu, Scr. Mater. 58 (2008) 122–125.

[16] J.J. Jonas, S.J. Mu, T.A. Samman, G. Gottstein, L. Jiang, E. Martin, Acta Mater. 59 (2011) 2046–2056.

[17] S.J. Mu, J.J. Jonas, G. Gottstein, Acta Mater. 60 (2012) 2043–2053.

[18] S. Mahajan S. Acta Metall. 21 (1973) 255.

[19] M. Niewczas, Acta Materialia 58 (2010) 5848–5857.

[20] W.B. Hutchinson, M.R. Barnett, Scripta Materialia 63 (2010) 737–740.

[21] J. Koike and R. Ohyama, Acta Mater. 53 (2005) 1963–1972.

[22] S. R. Agnew, C. N. Tome, D. W. Brown, T. M. Holden and S. C. Vogel, Scr. Mater. 48 (2003) 1003–1008.

Ref: Bunge's book (in appendix B)

[23] H.J. Bunge Mathematische methoden de texturanalyse. Berlin: Academic-Verlag; 1982.